Journal of proteome research

pubs.acs.org/jpr

Article

Quantitative Proteomics Reveal an Altered Pattern of Protein Expression in Brain Tissue from Mice Lacking GPR37 and GPR37L1

TrangKimberly Thu Nguyen, Eric B. Dammer, Sharon A. Owino, Michelle M. Giddens, Nora S. Madaras, Duc M. Duong, Nicholas T. Seyfried, and Randy A. Hall*

Cite This: *J. Proteome Res.* 2020, 19, 744−755

Read Online

ACCESS | Metrics & More | Article Recommendations | Supporting Information

ABSTRACT: GPR37 and GPR37L1 are glia-enriched G protein-coupled receptors that have been implicated in several neurological and neurodegenerative diseases. To gain insight into the potential molecular mechanisms by which GPR37 and GPR37L1 regulate cellular physiology, proteomic analyses of whole mouse brain tissue from wild-type (WT) versus GPR37/GPR37L1 double knockout (DKO) mice were performed in order to identify proteins regulated by the absence versus presence of these receptors (data are available via ProteomeXchange with identifier PXD015202). These analyses revealed a number of proteins that were significantly increased or decreased by the absence of GPR37 and GPR37L1. One of the most decreased proteins in the DKO versus WT brain tissue was S100A5, a calcium-binding protein, and the reduction of S100A5 expression in KO brain tissue was validated via Western blot. Coexpression of S100A5 with either GPR37 or GPR37L1 in HEK293T cells did not result in any change in S100A5 expression but did robustly increase secretion of S100A5. To dissect the mechanism by which S100A5 secretion was enhanced, cells coexpressing S100A5 with the receptors were treated with different pharmacological reagents. These studies revealed that calcium is essential for the secretion of S100A5 downstream of GPR37 and GPR37L1 signaling, as treatment with BAPTA−AM, an intracellular Ca^{2+} chelator, reduced S100A5 secretion from transfected HEK293T cells. Collectively, these findings provide a panoramic view of proteomic changes resulting from loss of GPR37 and GPR37L1 and also impart mechanistic insight into the regulation of S100A5 by these receptors, thereby shedding light on the functions of GPR37 and GPR37L1 in brain tissue.

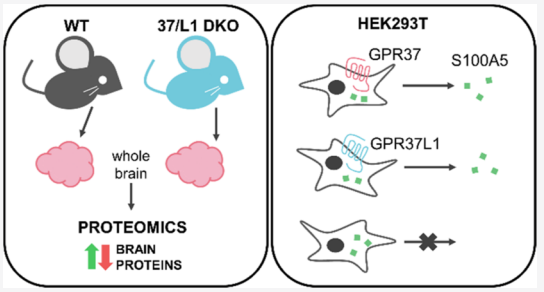

KEYWORDS: *S100A5, glia, calcium, secretion, astrocyte, oligodendrocyte, calcium-binding protein*

INTRODUCTION

GPR37 and GPR37L1 are closely related G protein-coupled receptors (GPCRs) that are highly expressed in the brain. These receptors exhibit differential expression in two distinct glial populations, with GPR37L1 being the most highly expressed in astrocytes and GPR37 being enriched in oligodendrocytes.[1−9] The first ligand reported for GPR37 was the invertebrate peptide known as head activator.[10,11] Subsequently, the secreted vertebrate protein prosaposin and its active fragment prosaptide were reported to bind and activate both GPR37L1 and GPR37.[12] Activation of GPR37 and/or GPR37L1 by prosaptide has been corroborated by several other groups,[2,13−15] although several reports have also failed to detect significant activation of these receptors by prosaptide.[16,17] Recent work by Liu et al. suggested a resolution of these seemingly disparate findings by providing evidence that prosaptide stimulation of GPR37 and GPR37L1 is dependent on cellular context, being readily observed in primary cells such as astrocytes but more difficult to observe in heterologous cells over-expressing the receptors.[2] Additionally, the bioactive lipid neuroprotectin D1 has also recently been reported as a ligand for GPR37.[13] Thus, despite the recent progress, more work is still needed to achieve a consensus as to the endogenous ligand(s) for GPR37 and GPR37L1.

Much of the current understanding of GPR37 and GPR37L1 function stems from studies that have focused on characterizing mice lacking the expression of one or both receptors. Knockout of GPR37 has been linked to altered dopamine signaling,[18] precocious oligodendrocyte differentiation,[7] and increased susceptibility to demyelination,[5] whereas knockout of GPR37L1 has been linked to precocious cerebellar development[19] and enhanced seizure vulnerability.[20] Moreover, mutations in GPR37L1 in humans have been associated with seizures and epilepsy.[20,21] The link between GPR37L1 and changes in seizure susceptibility in both humans and mice is intriguing, given the predominant expression of GPR37L1 in astrocytes and the fact that most epilepsy-associated proteins are mainly expressed in neurons.[22]

Received: September 12, 2019
Published: January 5, 2020

https://dx.doi.org/10.1021/acs.jproteome.9b00622
J. Proteome Res. 2020, 19, 744−755

The phenotypes observed in mice lacking GPR37 and GPR37L1, as well as the links between GPR37L1 variants and human disease, have led to interest in achieving a better understanding of the roles these receptors play in regulating cellular and molecular processes in the brain. Here, we utilized a proteomic approach to study the effect of knocking out GPR37 and GPR37L1 on global protein expression in the mouse brain. Insights gained from these studies can lead to a better understanding of the processes and molecular mechanisms regulated by GPR37 and GPR37L1 and thereby help to guide future studies on these glia-enriched receptors.

MATERIALS AND METHODS

Animals

GPR37L1 knockout mice ($Gpr37l1^{-/-}$) were obtained from the NIH Mutant Mouse Regional Centers (strain $Gpr37l1^{tm1Lex}$, stock number 011709-UCD) and GPR37 knockout mice ($Gpr37^{-/-}$) were obtained from Jackson Laboratories (strain $Gpr37^{tm1Dgen}$, stock number 005806). The double knockout mouse ($Gpr37^{-/-}$ and $Gpr37l1^{-/-}$) was made by crossing $Gpr37^{-/-}$ and $Gpr37l1^{-/-}$ mice, and genetic deletion of both genes was confirmed via DNA sequencing. All mice were maintained on a C57BL/6J background and housed on a 12 h light/dark cycle with food and water ad libitum. All experiments were done in accordance with the guidelines of the Institutional Animal Care and Use Committee of Emory University.

Tissue Preparation for Proteomic Analysis

Proteomic data were generated as stated by Smith et al. (2017).[5] Brain lysates were prepared from 3 month old WT (n = 3) and GPR37L1/GPR37 double knockout (DKO) mice (n = 3) in urea buffer (8 M urea, 100 mM $NaHPO_4$, pH 8.5) with HALT protease and phosphatase inhibitor (Pierce) and processed at the Emory Proteomics Core. An aliquot of 100 μg from each sample was treated with 1 mM (final concentration) dithiothreitol (DTT) for 30 min followed by 5 mM (final concentration) iodoacetamide for 30 min in the dark. Both steps were performed at room temperature. The protein mixtures were digested with 1:100 (w/w) lysyl endopeptidase (Wako) at 25 °C for 2 h. Trypsin (Promega) was then added at 1:50 (w/w), and digestion was allowed to proceed overnight. Resulting peptides were desalted with a Sep-Pak C18 column (Waters) and dried under vacuum.

Liquid Chromatography Coupled to Mass Spectrometry

Dried peptides were resuspended in peptide 100 μL of loading buffer (0.1% formic acid, 0.03% TFA, 1% acetonitrile). Peptide mixtures (2 μL) were separated on a self-packed C18 (1.9 μm Dr. Maisch, Germany) fused silica column (25 cm × 75 μm internal diameter (ID); New objective, Woburn, MA) using a Dionex UltiMate 3000 RSL CNano and monitored on a Fusion mass spectrometer (Thermo Fisher Scientific, San Jose, CA). Elution was performed over a 140 min gradient at a rate of 300 nL/min with buffer B ranging from 3 to 99% (buffer A: 0.1% formic acid in water, buffer B: 0.1% formic acid in acetonitrile). The gradient starts off at 3% B and goes to 10% within 5 min, then from 10 to 40% within 100 min, then from 40 to 60% within 20 min, then from 60 to 99% in 5 min, and finally settling at 99% for the rest of the gradient. The mass spectrometer cycle was programmed to collect at the top speed for 3 s cycles. The spray voltage starts off at 2 kV and changes to 2.2 kV at 75 min. The MS scans (400−1500 m/z range, 200,000 AGC, 50 ms maximum ion time) were collected at a resolution of 120,000 at m/z 200 in profile mode. The higher energy dissociation MS2 spectra (1.6 m/z isolation width, 0.5 m/z offset, 32% collision energy, 10,000 AGC target, 35 ms maximum ion time) were detected in the ion trap in the centroid mode. Dynamic exclusion was set to exclude previous sequenced precursor ions for 30 s within a 10 ppm window. Precursor ions with +1 and +8 or higher charge states were excluded from sequencing.

Database Search and Label-Free Quantification

The raw liquid chromatography/mass spectrometry (LC/MS/MS) data were then analyzed via MaxQuant v1.5.4.1 using Andromeda search employing a target-decoy paradigm to control the MS/MS peptide spectral match false discovery rate (FDR) and a database of contaminants plus the mouse Uniprot database (n = 54,489 protein isoforms, downloaded April 2015). MaxQuant search parameters allowed up to two miscleavages, fully tryptic peptides only, and fixed modification of cysteine by carbamidomethylation (+57.0215 Da), plus variable oxidation of methionine (+15.9949 Da) and protein N-terminal acetylation (+42.0106 Da). Other search settings included a maximum peptide mass of 4,600 Da, a minimum peptide length of 7 residues, and 0.05 Da tolerance for high resolution MS/MS scans. Cofragmented peptide search was enabled to deconvolute multiplex spectra. The FDR for peptide spectral matches, proteins, and site decoy fraction were all set to 1%. The "match between runs" function was used to recover unsequenced precursors. Matches were matched within a 0.7 min retention time match window and a 20 min alignment. Quantitation of proteins was performed using label-free quantitation (LFQ) with consideration of only razor and unique peptides. The MS proteomics data have been deposited to the ProteomeXchange Consortium via the PRIDE[24] partner repository with the dataset identifier PXD015202.

Data Processing and Determination of Differential Protein Abundance in DKO Versus Wild-Type

Because data-dependent acquisition and LFQ can miss individual sample measurements with a left-censoring (informative missingness) bias, the LFQ intensity quantitative data from MaxQuant for the n = 6 samples were filtered to limit missingness, and then, missing values were imputed, as previously described.[25−27] Imputation of missing protein LFQ intensity values was performed using the imputation algorithm of Perseus[27] as implemented in R and previously reported.[25] Proteins were considered to have a detectable fold change (FC) if the FC was a minimum of $\log_2(1.286)$, 28.6% or more, represented by $\log_2$(DKO/WT) values of −0.36 and 0.36 or for downregulated and upregulated proteins, respectively. This threshold for FC was determined, as described in the below section. Significant differentially expressed proteins were then determined by additional filtering for t-test p values less than 0.05. In addition, any proteins that were sequenced and quantified on one unique or razor peptide maximum in any of the six samples were excluded.

Filtering of Quantitative Results (after Imputation of Missed Quantitation)

We removed 581/4512 proteins from consideration that were sequenced and quantified on one unique or razor peptide maximum in any of the six samples. We determined the distribution of a true null 3 × 3 experiment of $\log_2$FC values. Each sample of three DKO and three WT measurements was converted to a null measurement by subtracting each of the $\log_2$ protein measurements from a paired measurement within the

https://dx.doi.org/10.1021/acs.jproteome.9b00622
J. Proteome Res. 2020, 19, 744−755

same genetic group, and then, the null WT average $\log_2$ protein abundance was subtracted from the null DKO average, as previously described.[29] The distribution histogram was fit to a Gaussian distribution as reported by Dammer et al., 2015,[29] where 1.96-fold of SD of the Gaussian fit to the histogram of the null 3931 measurements was $\log_2(1.286)$, or a minimum FC of 28.6%. The counting of proteins beyond 1.96-fold (SD) corresponds to false positive quantitative measurements in a 3-sample versus 3-sample comparison of WT null samples to DKO null samples that are expected to have no change. In the fit normal distribution, the relative area under the curve for the tails beyond this $\log_2$(FC) cutoff represents a probability of 0.05. At this FC cutoff, the null test produces 156/3931 (3.9%) of measurements that pass the FC criteria. This indicates that data filtered for minimum percent change 28.6% have been controlled to an empirical FDR of less than 4%. Additional FDR calculations were performed in R via Perseus' (v1.6.10.43) edgeR implementation for determination of differential expression with FDR using default options of 0.04 dispersion factor, generalized linear modeling, and no additional normalization of LFQ abundances, non-log transformed. In addition, an *R* implementation of *T*-test permutation with 10,000 iterations for each protein using the independence test function of the R coin package run in R v3.5.2 generated permutation-based FDR values for all $N = 3931$ proteins with at least 2 peptides quantified as $\log_2$(LFQ abundance). All protein measurements used were devoid of missing values following imputation, as described. The R code is available upon request.

Cell Culture and Cellular Transfection

Human embryonic kidney cells (HEK293T cells) (ATCC) were maintained in complete media [Dulbecco's modified Eagle's medium (DMEM) 1× (Life Technologies) supplemented with 10% fetal bovine serum (Atlanta Biologicals) and 1% penicillin/streptomycin (Quality Biological)] in a humid, 5% CO_2, 37 °C incubator. Cells were plated at 40% confluence the day prior to transfection. For standard transfections, 2 μg of each DNA construct was used for a total DNA amount of 4 μg per 10 cm plate. Transfections were done using Mirus TransIT-LT1 (Madison, WI) according to manufacturer's protocol. Following transfection, cells were incubated for 48 h prior to harvesting. Constructs used included the following: empty vector, human GPR37L1 (untagged), human GPR37 (untagged), human S100A5-myc-DDK (Origene), human S100A4-myc-DDK (Origene), and human S100A6-myc-DDK (Origene).

Cell Lysate Preparation

Cells were lysed and harvested in low-salt harvest buffer (10 mM HEPES (pH 7.3), 50 mM NaCl, 5 mM EDTA in ultrapure water) + HALT protease, and phosphatase inhibitor (Thermo Fisher) (1% Triton X-100 was added to the low-salt harvest buffer if cells were solubilized). For solubilization, cells were rotated end-over-end at 4 °C for at least 1 h and then spun down at 15,000 rpm for 15 min to pellet. Laemmli sample buffer was added to cell lysate samples and left at room temperature overnight to prepare for Western blot analysis.

Western Blot Analyses

Protein samples were reduced and denatured in Laemmli buffer and analyzed via SDS-PAGE. Samples were loaded onto 4−20% Tris-glycine gels (Bio-Rad) and then transferred to nitrocellulose membranes (Bio-Rad). For analysis via chemiluminescence, membranes were blocked in 5% milk (5% nonfat milk in 50 mM NaCl, 10 mM HEPES, pH 7.3, 0.1% Tween-20 (Sigma) in ultrapure water) and then incubated with primary antibodies, shaking overnight at 4 °C. For analysis via infrared fluorescent Western detection, membranes were blocked with Odyssey Blocking Buffer (Licor) for 1 h at room temperature and then incubated with primary antibodies, shaking overnight at 4 °C as per manufacturer's protocol. Membranes were then washed three times for 5 min each with wash buffer (1× PBS + 0.1% Tween-20) and then incubated with secondary antibodies that were diluted in blocking buffer. Membranes were again washed three times for 10 min each with wash buffer and were then imaged using the ChemiDoc Gel Imaging System. Protein quantification was done with ImageJ.

Secretion Analyses

Transfected HEK293T cells were incubated in complete media (DMEM 1× + 10% FBS + 1% penicillin/streptomycin) for 48 h and media were collected on the day of harvesting, and HALT protease and phosphatase inhibitor (Thermo Scientific) were added to each media sample. Because the S100A protein constructs are all myc- and FLAG-tagged, myc-A/G agarose beads were used to pull down S100A proteins from the media. To pull down any S100A protein that may have been secreted into the media, each medium sample was incubated with 60 μL (a nonsaturated volume) of washed myc-A/G agarose bead slurry (Thermo Scientific) and rotated end-over-end at 4 °C for 2 h. Beads were then washed three times with low-salt harvest buffer, and 2× Laemmli sample buffer was added to each bead sample and incubated at room temperature overnight prior to Western blot analysis.

For signaling studies, BAPTA−AM (Sigma-Aldrich), an intracellular calcium chelator, and prosaptide (TX14(A)) (Tocris Bioscience), a reported ligand for GPR37 and GPR37L1, were reconstituted to a stock concentration in the appropriate solvent. Cells were treated with compounds 24 h after transfection and overnight prior to harvesting for protein and secretion analyses.

RNA Extraction and cDNA Conversion

Total mRNA was extracted from brain tissues and converted to cDNA for real-time quantitative polymerase chain reaction (RT-qPCR). Tissues were collected in 500 μL of TRIzol and dissociated by trituration. TRIzol mixtures were allowed to incubate at room temperature for 5 min. Following incubation, 100 μL of chloroform was added to each sample and tubes were shaken vigorously by hand for about 15 s to ensure thorough mixture. Samples were then allowed to incubate at room temperature for 5 min and then centrifuged at 15,000 rpm at 4 °C for 15 min. The top, clear aqueous layer was collected into a new Eppendorf tube (about 200 μL in volume), 250 μL of isopropyl alcohol was added to each sample, and samples were inverted several times to ensure mixing. Samples were then incubated at room temperature for 10 min and centrifuged at 15,000 rpm at 4 °C for 10 min to pellet the RNA. The supernatant was removed using a pipette, and the RNA pellet was washed with 500 μL of 75% ethanol three times, spinning down at 15,000 rpm at 4 °C for 5 min in between each wash. Following the final wash, the RNA pellet was allowed to dry on the benchtop at room temperature for 10−15 min or until most of the ethanol had evaporated. RNA pellets were then resuspended in RNAse-free water and incubated at 55 °C for 10 min to rehydrate. RNA was stored at −80 °C when not being used.

RNA was converted to cDNA via reverse transcription polymerase chain reaction (RT-PCR). Each RNA sample was

https://dx.doi.org/10.1021/acs.jproteome.9b00622
J. Proteome Res. 2020, 19, 744−755

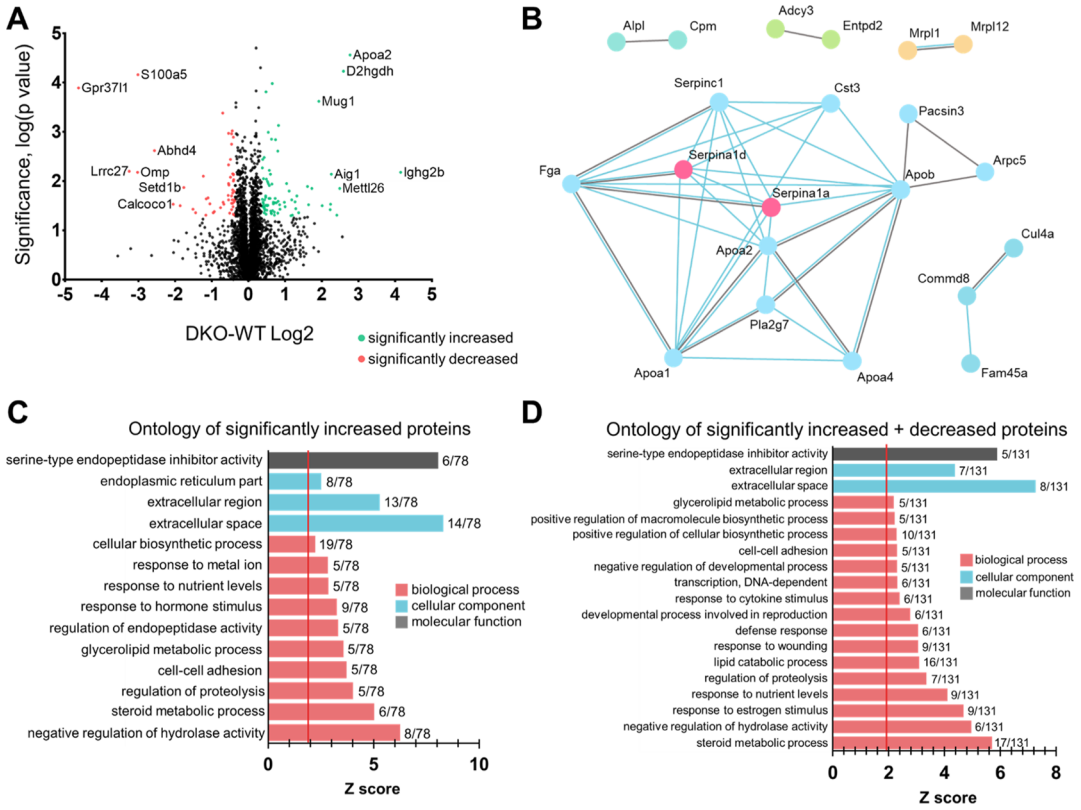

Figure 1. Imputation and analysis of proteomic data. (A) Volcano plot depicting all protein hits from proteomic analyses, comparing global protein changes between DKO and WT mouse brains. Whole mouse brain lysates were processed at the Emory Proteomics Core for analysis via MS. *x*-axis represents FC (increased, positive $\log_2$(DKO/WT) or decreased, negative $\log_2$(DKO/WT)) and the *y*-axis represents $-\log_{10}(p$ value), that is, the bigger the $-\log_{10}(p$ value), the more significant the data point is. Proteomic screen yielded only a small handful of proteins that exhibited both a significant and high FC. Data points colored in red are those proteins that were significantly decreased ($p \leq 0.05$, DKO−WT $\log_2 \leq -0.36$) in DKO mouse brains compared to WT mouse brains, and data points colored in green are those that were significantly increased ($p \leq 0.05$, DKO−WT $\log_2 \geq 0.36$). Out of over 4,500 proteomic hits, only 78 were significantly increased (greater than or equal to +28.6% FC) and only 53 were significantly decreased (less than or equal to −28.6% FC) when both GPR37 and GPR37L1 were knocked out. WT, $n = 3$; DKO, $n = 3$. (B) Protein−protein interaction network between the 78 increased and 53 decreased proteins was generated via STRING analysis (string-db.org). This network identifies any protein−protein interactions determined experimentally (blue lines) or found in curated databases (gray lines). (C, D) Ontology graphs were generated each for the increased (C) and increased and decreased combined (D) lists of proteins.

diluted to 2−5 μg and incubated with 1 μL of 10 mM dNTPs, 0.5 μL of random primers (50 ng/μL), and 5.5 μL of DEPC dH_2O at 65 °C for 5 min. This RNA mixture was then incubated with 4 μL of 5X RT Buffer (Thermo Fisher), 2 μL of 0.1 M DTT, 1.5 μL of DEPC dH_2O, 0.25 μL of RNaseOUT, and 0.25 μL of SuperScript III RT (Thermo Fisher) at room temperature for 10 min and then incubated at 42 °C for 50 min.

Quantitative Polymerase Chain Reaction

cDNA made from the above protocol was used for quantitative analysis of mRNA expression in cell and tissue samples via the Bio-Rad Thermo Cycler C1000 Touch system using the DyNAmo ColorFlash SYBR Green qPCR kit (Thermo Fisher). Each reaction was performed in triplicate, and the following thermal cycle protocol was used for all reactions: (1) 95 °C for 7 min, (2) 95 °C for 10 s, (3) 60 °C for 30 s, 40 cycles, steps 2−3, and (4) melting curve obtained according to the instrument manufacturer. The following primers were made and purchased from Eurofins Genomics: GAPDH forward: 5′-ACC ACA GTC CAT GCC ATC AC-3′; GAPDH reverse: 5′-TCC ACC ACC CTG TTG CTG TA-3′; S100A5 forward: 5′-GCA AGC TGA CCC TGA GTA GG-3′; S100A5 reverse: 5′-CGC TGT TTT TGT CCA GGC TC-3′. Data were analyzed via the ΔΔCT method described previously,[30] and results are expressed as relative expression normalized to wild-type (WT) samples.

Antibodies Used

PRDX6 (Cell Signaling Technologies) WB 1:1000; EBP (Invitrogen) WB 1:1000; S100A5 (Novus) WB 1:5000; GAPDH (Millipore) WB 1:5000; Flag-HRP (Invitrogen) WB 1:5000; GPR37L1 (Mab Technologies) WB 1:2000; GPR37 (Mab Technologies) WB 1:2000; IRDye 680LT goat antichicken (Licor) WB secondary antibody 1:2000; IRDye 800LT goat antirabbit (Licor) WB secondary antibody 1:2000.

S100A5 Antibody Validation

Lysates from HEK293T cells that were transfected with either S100A4-mycDDK (Origene), S100A5-mycDDK (Origene), or S100A6-mycDDK (Origene) were used for validation of S100A5 antibody specificity. Samples were prepared for Western blot as mentioned above, and Western blot analysis was performed. Membranes were blotted with S100A5 (Novus, 1:5000) to check for specificity, and Flag-HRP (Invitrogen, 1:5000) to confirm that all three constructs were present in the samples (Supporting Information Figure S4).

https://dx.doi.org/10.1021/acs.jproteome.9b00622
J. Proteome Res. 2020, 19, 744−755

Table 1. Top Seven Most Significantly Decreased Proteins in DKO Versus WT Whole Mouse Brain Identified via MS

uniprot ID	gene symbol	percent decrease, LFQ signal (%)	*T*-test *p* value ▲	traditional FDR (Benjamini–Hochberg) (%)	max single-sample razor + unique peptide counts	
					DKO	WT
P63084	S100a5	−88	6.94×10^{-5}	5.4	0	3
Q99JG2	Gpr37l1	−96	1.27×10^{-4}	6.6	0	3
P20917	Mag	−38	4.16×10^{-4}	11.8	14	15
P47199	Cryz	−26	9.62×10^{-4}	18.2	8	10
P52760	Hrsp12	−31	1.07×10^{-3}	18.2	8	9
P21460	Cst3	−27	1.11×10^{-3}	18.2	5	5
Q8VDK1-2	Nit1	−24	1.30×10^{-3}	18.2	9	9

Table 2. Top Nine Most Significantly Increased Proteins in DKO Versus WT Whole Mouse Brain Identified via MS

uniprot ID	gene symbol	percent increase, LFQ signal (%)	*T*-test *p* value ▲	traditional FDR (Benjamini–Hochberg) (%)	max single-sample razor + unique peptide counts	
					DKO	WT
P09813	Apoa2	581	2.73×10^{-5}	5.3	2	3
Q8CIM3	D2hgdh	501	5.85×10^{-5}	5.4	5	0
Q91XF0	Pnpo	56	1.05×10^{-4}	6.6	4	3
Q91V76	4931406C07Rik	40	1.53×10^{-4}	6.6	8	8
P28665	Mug1	279	2.42×10^{-4}	9.2	16	7
Q00623	Apoa1	77	7.39×10^{-4}	18.2	14	14
Q65CL1	Ctnna3	46	1.02×10^{-3}	18.2	4	3
Q00897	Serpina1d	55	1.40×10^{-3}	18.3	3	2
Q9DB15	Mrpl12	67	1.44×10^{-3}	18.3	3	3

RESULTS

Proteomic Analysis of Global Protein Changes in the DKO Mouse Brain Versus WT Mouse Brain

To gain insight into the potential physiological actions of GPR37 and GPR37L1 in the brain, MS-based label-free proteomics was performed on whole mouse brain lysates. Because the seizure phenotype is most severe in the DKO mice, the proteomic screen was performed on WT and DKO mouse brains to assess whether the levels of certain proteins were altered by the loss of these two related GPCRs. Samples of WT and DKO whole brain lysates from adult (3 month old) mice were prepared in urea lysis buffer, as previously described,[23] and submitted to the Emory Integrated Proteomics Core for proteomic analyses via LC/MS. In total, 4,512 unique proteins were identified in the proteomic analyses between the six total WT and DKO mouse brain lysates.

The LFQ dataset was imputed using the imputation algorithm of Perseus to address the missing values according to an assumption of informative missingness, and 581 proteins from the original list were not considered because of unreliable, single peptide, measurement or high missingness of protein quantitation across the six measurements (Supporting Information S1). Then, differentially expressed proteins between WT and DKO samples ($n = 3$ each) were determined, as described in the Materials and Methods, under using filtering criteria specified in the section "Filtering of quantitative results (after Imputation of Missed Quantitation)" and are represented as either red or green dots on a volcano plot (Figure 1A). Red points on the volcano plot represent proteins with significant negative FC, and green points represent proteins with significant positive FC. Empirical FDR based on the true null 3 × 3 experiment indicates an FDR of <4% without one-peptide identifications. Through determination of the distribution of a null experiment fit to a Gaussian distribution, data were filtered for a minimum percent change of 28.6% and a *p* value equal to or less than 0.05 (calculations for the null experiment and FDR can be found in Supporting Information S2). Based on these criteria, the vast majority of proteins did not exhibit any significant changes in expression between WT and DKO brain tissues. However, out of over 4,500 proteins identified and quantified, a small handful of proteins was found to exhibit differential expression, with 78 proteins found to be significantly increased and 53 found to be significantly decreased (the full tables of significantly increased and decreased proteins can be found in Supporting Information S3). These differentially expressed proteins were then analyzed via GO-Elite "biological process," "cellular component," and "molecular function" categorical annotation using DAVID to identify the most enriched pathways and/or functions of either increased proteins (Figure 1C) or increased and decreased proteins combined (Figure 1D; the full list of proteins found for each ontology can be found in Supporting Information S4). No ontologies were identified for the list of decreased proteins alone. A Z score of 1.96 or greater represented a functional enrichment or overrepresentation by Fisher's Exact test that was significant within the given protein list. For increased proteins as well as the increased and decreased proteins combined, the only major enriched biological process was serine-type endopeptidase inhibitor activity (Z score = 8.07 and 5.88, respectively). For "cellular component," extracellular space and extracellular region were overrepresented with *Z* scores of 5.29 and 8.30, respectively, for only increased proteins and *Z* scores of 4.37 and 7.27, respectively, when analyzing both increased and decreased proteins together. For "molecular function," the top three functional enrichments found when

https://dx.doi.org/10.1021/acs.jproteome.9b00622
J. Proteome Res. 2020, 19, 744−755

looking at only increased proteins were "negative regulation of hydrolase activity," "steroid metabolic process," and regulation of proteolysis with Z scores of 6.25, 5.03, and 4.02, respectively. Some other interesting associations were found for other molecular functions, such as glycerolipid metabolic process and response to hormone stimulus.

When looking at ontologies for increased and decreased protein lists together, the top three enrichments in "molecular function" were "steroid metabolic process" (Z score = 5.70), "negative regulation of hydrolase activity" (Z score = 4.97), and "response to estrogen stimulus" (Z score = 4.68). Interestingly, "glycerolipid metabolic process" appears on both ontology analyses for only increased proteins as well as both increased and decreased protein lists combined. It should be noted that this direction of change is consistent with compensation for or responsiveness to accumulation of glycerolipids known to occur when saposins' function is compromised at the lysosome, and a reported ligand for both GPR37L1 and GPR37 is prosaptide, an active fragment of prosaposin, which is known to be involved in lysosomal trafficking and biology.[12,31−36] Additionally, a protein−protein interaction network was generated for the list of proteins that were significantly differentially expressed (both up and downregulated) (Figure 1B). Only proteins that had an interaction with at least one other protein were displayed.

Proteome-Wide Changes in the DKO Mouse Brain

The top decreased and increased proteins found in the proteomic analyses were used for further validation in in vitro studies (Tables 1 and 2). GPR37 and GPR37L1 have been reported to be expressed in distinct cell types and cell populations within the brain, with GPR37L1 being most highly expressed in astrocytes[1,14,19,37] and GPR37 being most abundantly expressed in oligodendrocytes.[1,7,38] Because of this cell-specific expression in the central nervous system, both the imputed lists for significantly increased and decreased proteins found via MS were analyzed for cell type expression to assess how knockout of both these receptors affected the cell type expression profile of proteins that were changed. Both lists were run against reported cell type-enriched expression databases via Differential Enrichment analysis of Proteomics data (DEP), including those reported by Sharma et al. (2015) and the Barres lab.[9,23,25,28] Fisher's exact test was performed and heatmaps were prepared, depicting −log(p-value). Interestingly, significantly upregulated proteins were found to be mostly expressed in neurons, microglia, and endothelial cells across the three different databases, while significantly downregulated proteins were found enriched mostly in astrocytes and oligodendrocytes (Supporting Information Figures S1−S3). The lists of proteins that were found for each cell type by each database and their corresponding FET values are shown in Supporting Information S5. Because GPR37 and GPR37L1 are most highly expressed in astrocytes and oligodendrocytes, respectively, we focused on proteins that were significantly decreased (Table 1).

The top five most significantly downregulated proteins included S100 calcium-binding protein A5 (S100A5), GPR37L1, myelin-associated glycoprotein (MAG), quinone oxidoreductase (CRYZ), and 2-iminobutanoate/2-iminopropanoate deaminase (HRSP12). We have previously published on the role of GPR37 knockout resulting in the downregulation of MAG.[5] Western blot analyses were performed to either confirm or refute the other top hits based on the proteomic data.

Western blot analysis revealed that there was a significant decrease of S100A5 across the single and DKO mouse brains compared to WT mouse brain. Expression of S100A5 was found to be reduced in KO mouse brain tissue by approximately 75−80% (Figure 2A, quantification Figure 2B), a reduction that is in line with the proteomic data. Levels of S100A5 mRNA in DKO versus WT mice were also analyzed. In line with the proteomic data and the Western blot data, mRNA levels of S100A5 were found by qPCR to be reduced about 75% in the DKO mouse brain. These data suggest that regulation of S100A5 by GPR37 and GPR37L1 occurs at least partially at the level of transcription.

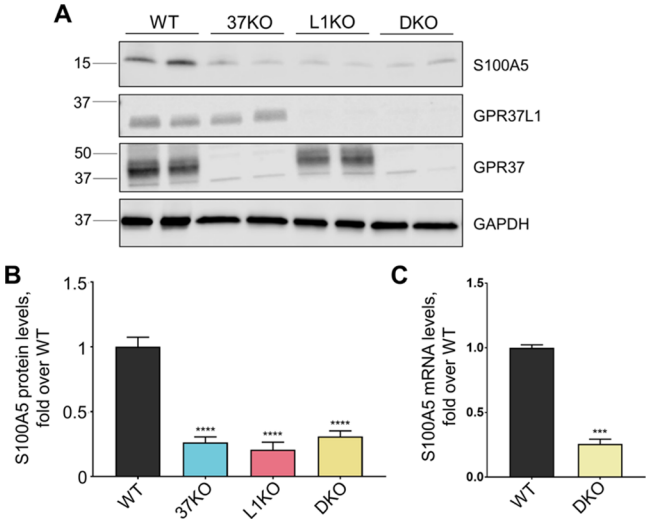

Figure 2. S100A5 protein and mRNA levels are reduced in GPR37 knockout, GPR37L1 knockout, and DKO mouse brains versus WT mouse brain. Representative Western blot depicting protein levels in whole mouse brain lysates. S100A5 is significantly downregulated in knockout mouse brains compared to WT mouse brains. (A) Western blots were quantified via ImageJ (B) (n = 7, ****p < 0.0001, bars represent SEM, one-way ANOVA, Dunnett's post-hoc). (C) S100A5 mRNA levels in WT vs DKO mouse brain (n = 4, ***p = 0.0003, student's t-test, bar represents SEM). All samples were normalized to GAPDH.

S100A5 Secretion is Regulated by GPR37 and GPR37L1 and is Receptor-Dependent

To further explore potential regulation of S100A5 by GPR37 and GPR37L1, we moved into a mammalian cell line. HEK293T cells were transfected with S100A5 in the absence and presence of either GPR37 or GPR37L1. As knockout of the receptors led to downregulation of S100A5 in vivo at the protein and transcript level, we assessed whether coexpression of S100A5 with either receptor might lead to upregulation of S100A5. However, there was little to no effect of the receptors on the total expression of S100A5 (Figure 3A), an observation consistent with the aforementioned qPCR data, suggesting that the effect of the receptors on S100A5 expression in vivo was mainly a result of transcriptional changes and not an effect on protein stability. Interestingly, though, we also analyzed media from transfected cells and found that S100A5 was only detectable in the media of cells in which S100A5 had been coexpressed with either GPR37 or GPR37L1. No detectable amounts of S100A5 were found in the condition in which S100A5 was expressed alone (Figure 3B). While there appeared to be somewhat more S100A5 secreted from cells coexpressing S100A5 and GPR37 compared to cells coexpressing S100A5 and GPR37L1, statistical analyses revealed that the amount of S100A5 secreted from those two conditions

https://dx.doi.org/10.1021/acs.jproteome.9b00622
J. Proteome Res. 2020, 19, 744−755

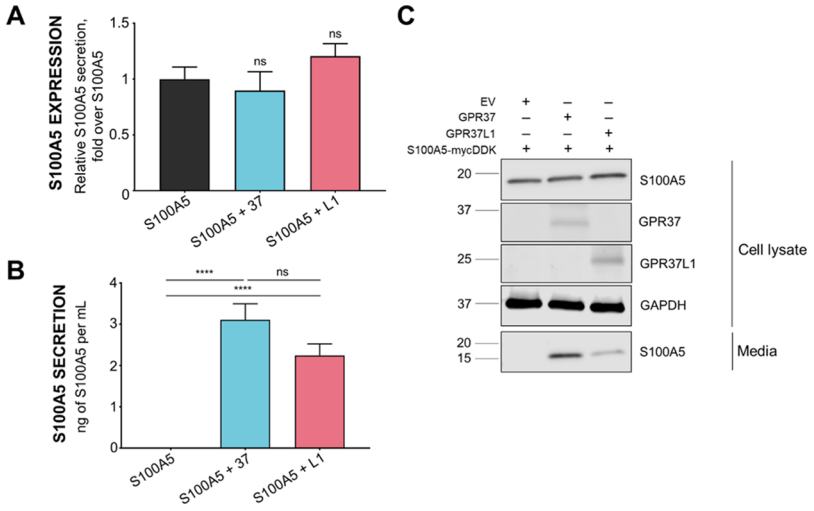

Figure 3. Coexpression of S100A5 with either GPR37 or GPR37L1 leads to robust secretion of S100A5 from HEK293T cells. (A) Coexpression of S100A5 with either GPR37 or GPR37L1 in HEK293T cells did not significantly increase intracellular S100A5 expression (n = 12 per condition, bars represent SEM, one-way ANOVA). (B) Coexpression of S100A5 with either GPR37 or GPR37L1 did increase S100A5 secretion compared to S100A5 expression alone (n = 7, bars represent SEM one-way ANOVA, ****: $p < 0.0001$). (C) Representative Western blot of cell lysates and media is shown on the right, demonstrating expression of transfected proteins (cell lysate) and secretion (media) of S100A5 into the media. HEK293T cells were transfected to coexpress S100A5 in the absence and presence of GRP37 or GPR37L1.

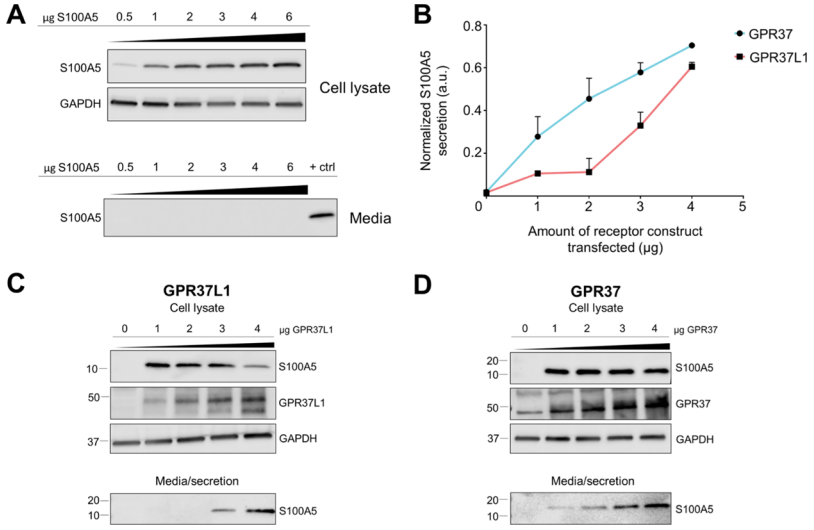

Figure 4. Receptor regulation of S100A5 secretion. (A) To assess whether secretion of S100A5 can be induced by simply overexpressing the protein, increasing amounts of S100A5 plasmid (0.5 μg up to 6 μg) were transfected into HEK293T cells. However, increasing S100A5 levels in HEK293T cells did not lead to detectable S100A5 secretion, suggesting that secretion of S100A5 is receptor-dependent. (B) Secretion of S100A5 increased according to the amount of receptor coexpressed (this panel shows a quantification of the data shown in panels C and D). (C) Representative Western blot depicting the effect of increasing GPR37L1 levels on S100A5 secretion (n = 4). (D) Representative Western blot depicting the effect of increasing GPR37 levels on S100A5 secretion (n = 4). All samples were normalized to GAPDH. Bars represent SEM.

was not significantly different. These data suggested that the presence of the receptors was able to induce secretion of S100A5 in transfected cells.

S100A proteins are known to be secreted, but almost nothing is known about the mechanisms regulating this secretion.[39] Thus, we performed further studies to investigate the role of GPR37 and GPR37L1 in the regulation of the secretion of S100A5. To rule out that S100A5 secretion was indiscriminate or because of simple overexpression of the protein, cells were transfected with increasing amounts of the S100A5 construct in the absence of the receptors, and intracellular expression and extracellular secretion of S100A5 into the media were analyzed. Western blot analyses revealed that even at 6 μg of S100A5 construct transfected, three times the amount normally transfected into cells, there was no detectable secretion of S100A5 by the cells (Figure 4A). Additionally, when the receptor constructs were transfected in increasing amounts (0–4 μg) and coexpressed with a constant amount of S100A5 construct (2 μg), there were receptor-dependent increases in the amount of secreted S100A5 (Figure 4C,D), with receptor expression levels exhibiting a positive linear relationship to the amount of S100A5 secreted (Figure 4B). There were no statistically significant differences in S100A5 secretion between the two conditions at any receptor concentration.

https://dx.doi.org/10.1021/acs.jproteome.9b00622
J. Proteome Res. 2020, 19, 744–755

Calcium Mediates S100A5 Secretion Downstream of GPR37L1 and GPR37 Constitutive Signaling

In further work, we investigated the mechanism by which GPR37 and GPR37L1 were able to enhance S100A5 secretion. HEK293T cells were transfected with S100A5 in the absence or presence of GPR37 or GPR37L1 and treated with increasing concentrations of BAPTA−AM, an intracellular Ca^{2+} chelator, or prosaptide (TX14A), a reported ligand for GPR37 and GPR37L1.[2,12,15] Interestingly, when HEK293T cells coexpressing S100A5 with either receptor were treated with increasing concentrations of BAPTA−AM, there were significant reductions in S100A5 secretion (Figure 5B,C). In contrast, treatment of transfected HEK293T cells with 100 nM prosaptide had no effect on S100A5 secretion (Figure 5A).

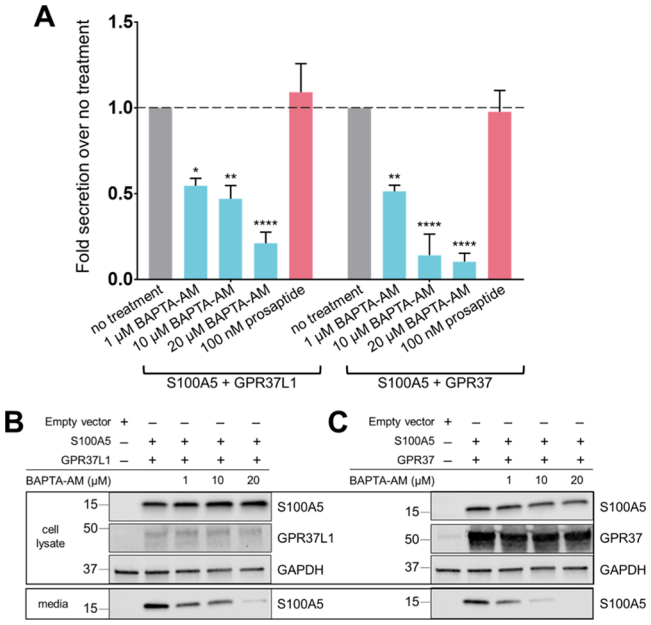

Figure 5. Chelation of intracellular Ca^{2+} leads to decreased S100A5 secretion from HEK239T cells. To elucidate the mechanism regulating S100A5 secretion, HEK293T cells were transfected with S100A5 and either GPR37 or GPR37L1. Cells were allowed to incubate for 24 h following transfection and then treated with different pharmacological reagents. (A) Normalized quantification of S100A5 secretion when cells were treated with either BAPTA−AM or the putative GPR37L1 ligand prosaptide (TX 14A) compared to transfected cells that did not receive treatment. (B) Representative Western blots depicting effects of increasing concentrations of BAPTA−AM on S100A5 secretion in cells coexpressing S100A5 and GPR37L1. (C) Representative Western blot depicting effects of increasing concentrations of BAPTA−AM on S100A5 secretion in cells coexpressing S100A5 and GPR37. (n = 3−4, bars represent SEM, two-way ANOVA within groups, Dunnett's post hoc) (*p = 0.0110; **p < 0.006; ****p < 0.0001).

Receptor-Mediated Secretion is Restricted to Homologous S100A Proteins

To assess whether this GPR37- and GPR37L1-mediated S100A5 secretion was specific only to S100A5 or was general for other members of the S100A protein family, we performed the same experiments with S100A4 and S100A10. These two proteins were not found to be significantly changed in the proteome. S100A4 is a protein of the S100A protein family that is closely related to S100A5, sharing 53% protein sequence identity and 70% sequence similarity. S100A10 is more distally related, sharing only 33% protein sequence identity and 62% sequence similarity (positives, BLAST of human protein sequences). Additionally, on phylogenetic trees constructed by sequence alignments of the S100 protein family, S100A4 and S100A5 are grouped in the same subgroup, with S100A10 found in a distinct subgroup.[39]

HEK293T cells were transfected to express either S100A4 or S100A10 in the absence or presence of GPR37 or GPR37L1, and expression and secretion of the S100A proteins were analyzed. When S100A4 was coexpressed with either GPR37 or GPR37L1, S100A4 was detected in the media (Figure 6A), whereas no detectable S100A4 was found when S100A4 was expressed alone. In contrast, coexpression of S100A10 with either receptor did not lead to any detectable secretion in the media (Figure 6B). These data suggest that GPR37 and GPR37L1 can promote secretion of S100A proteins related to S100A5 but not all members of the S100A family.

DISCUSSION

Previous findings revealed that the GPR37 single knockout, the GPR37L1 single knockout, and the DKO mice exhibit increased susceptibility to induced seizures, with the DKO mice exhibiting the most pronounced susceptibility.[20] Our proteomic analyses revealed that the loss of both GPR37 and GPR37L1 in the mouse brain led to the global increase and decrease of a small handful of proteins. Ontology analyses of significantly increased and decreased proteins combined revealed that proteins are involved in several processes such as "response to estrogen stimulus," "steroid metabolic processes," "defense response," and "response to cytokine stimulation." "Defense response" and "response to cytokine stimulation" are intriguing, as it suggests that a subset of significantly differentially expressed proteins may be involved in controlling inflammatory responses. For "response to estrogen stimulus" and "steroid metabolic processes," the steroid and estrogen connections may be interesting avenues for further investigation, given the genetic links between GPR37L1 and epilepsy[20,21] and the vast literature on the role of sex steroids in modulating seizure vulnerability in both humans and rodent models.[40−46]

Another interesting finding was that the majority of the decreased proteins were found to be enriched in astrocytes and oligodendrocytes (the two cell types in which GPR37 and GPR37L1 are enriched), while many of the increased proteins were found to be enriched mainly in neurons, microglia, and endothelial cells. It is possible that knockout of both receptors leads to the decrease of this handful of proteins in the respective native cell types, astrocytes, and oligodendrocytes, and subsequent deficits in the function of astrocytes and/or oligodendrocytes then lead to upregulation of certain proteins found in other cell types. One of the most decreased proteins from the proteomic analyses, S100A5, was found via Western blot to be reduced by about 75−80% in single and DKO mouse brain lysates. Moreover, mRNA transcripts of S100A5 were reduced by about 75% in the DKO mouse brain, suggesting transcriptional downregulation of S100A5 upon the loss of GPR37 and GPR37L1. In parallel in vitro studies, we found that S100A5 levels were not affected by coexpression with GPR37 or GPR37L1, but surprisingly, we observed robust secretion of S100A5 into the media upon coexpression with either receptor. S100A5 is a brain-enriched EF-hand motif-containing calcium-binding protein that can bind Ca^{2+}, Zn^{2+}, and Cu^{2+}[47] and has been reported to be expressed in astrocytes,[48,49] the cell type in which GPR37L1 is most abundantly expressed.

https://dx.doi.org/10.1021/acs.jproteome.9b00622
J. Proteome Res. 2020, 19, 744−755

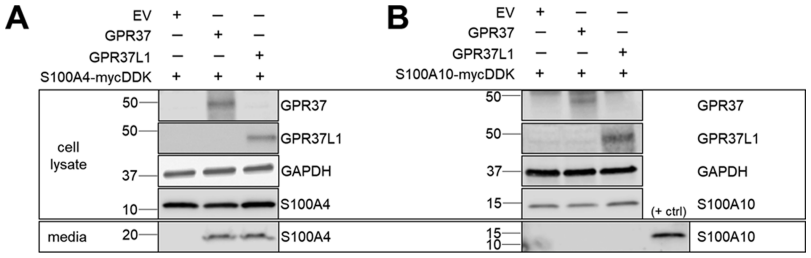

Figure 6. Coexpression of homologous S100A proteins with either GPR37L1 or GPR37 also leads to secretion. To explore whether GPR37- or GPR37L1-mediated secretion was specific only to S100A5 or general for other S100A protein family members, we examined whether coexpression of either GPR37 or GPR37L1 with S100A4 or S100A10 in HEK293T cells might lead to secretion of these proteins. (A) S100A4 coexpression with either receptor resulted in detectable secretion. (B) In contrast, S100A10 secretion was not observed upon coexpression with either receptor. The positive control shown here was a media sample containing secreted S100A5.

Little is known about the biological function of S100A5, but there has been a significant amount of work on other members of the S100A family. For example, the closely-related S100A4 was found to be upregulated in astrocytes in models of traumatic brain injury and kainic acid excitotoxicity, and it is also known to be secreted to act as a neuroprotective and neurotrophic factor.[50] Additionally, S100A6, another member of the S100A protein family that is highly homologous to S100A5, has also been reported to be secreted and regulated by pathological states.[51−53] Over the years, a number of reports have described roles for S100 calcium-binding proteins in the regulation of ion channels and neuronal excitability. In a study done by Kubista et al., extracellular application of either S100B or S100A1 to Helix neurons led to hyperpolarization of the membrane resting potential and inhibited spontaneous discharge activity of action potentials because of the effects on potassium channels.[54] Several other studies also describe effects of manipulation of extracellular S100 proteins (with antiserum or antibodies against S100 proteins, or treatment with S100 proteins) on neuronal activity.[55−58] Yet another study showed that secretion of S100B from astrocytes was dependent on presynaptic release of neurotransmitter.[59] Taken together, these studies provide evidence that S100 proteins can be secreted in response to neuronal activity and imply an extracellular modulatory function of S100 proteins on neuronal excitability. Therefore, it is conceivable that alterations in GPR37- or GPR37L1-mediated regulation of S100A5 could lead to altered neuronal activity and/or excitability and thereby contribute to the seizure susceptibility phenotype observed in mice lacking these receptors.

The molecular mechanisms by which S100A proteins are secreted are completely unclear. Serotonin receptor agonists, glutamate, lipopolysaccharide, changes in extracellular Ca^{2+} and K^{+}, and metabolic stress have all been reported to stimulate the release of S100 proteins from astrocytes.[60−63] Some studies suggest that secretion of S100 proteins may be passive or involve direct interaction with the plasma membrane.[64,65] Our work provides additional mechanistic insight into the secretion of S100A proteins, as we found that coexpression with GPR37 or GPR37L1 promoted the secretion of both S100A5 and S100A4. As these S100A proteins bind calcium, and as GPR37 and GPR37L1 can increase calcium levels downstream of G protein coupling,[10,11,13] we also assessed whether intracellular Ca^{2+} levels can affect secretion of S100A5. We found that treatment of transfected HEK293T cells with an intracellular Ca^{2+} chelator, BAPTA−AM, dramatically reduced secretion of S100A5. In further studies, it would be interesting to explore whether changes in intracellular Ca^{2+} levels result in specific conformational changes in S100A5 that promote secretion or conversely exert general effects on the secretion machinery. Several studies show that S100 calcium-binding proteins exposed to high intracellular Ca^{2+} levels can bind Ca^{2+} and subsequently adopt a conformation that exposes hydrophobic sites that then enables them to bind target proteins or membranes.[66,67] Interestingly, S100 proteins have also been reported to be associated with synaptosomes, including several recent proteomic studies that reveal the presence of S100 proteins in the synaptosome.[68−70] Several other studies show that S100 proteins are able to form tight complexes with binding sites in synaptosomal particulate fractions in both time- and temperature-dependent manners[71−73] and are shown to also localize to the synaptosome in mouse brain cortex.[74,75] Additionally, two studies that investigated the localization of S100 proteins in synaptosomal fractions showed that divalent cations such as Ca^{2+} and Mg^{2+} were necessary for S100 proteins to interact directly with synaptosomes.[73,76] While these studies highlight the role of S100 proteins in the neuronal synaptosome, it is possible that the binding of Ca^{2+} can affect the function and/or secretion of S100 proteins from glial cells as well.

We also assessed the effect of prosaptide, a reported endogenous ligand for GPR37 and GPR37L1, on S100A5 secretion, but found no effect of prosaptide treatment. This may be due to several factors, including that GPR37 and GPR37L1 have both been reported to exhibit high levels of constitutive activity in transfected cells.[5,17] Moreover, recent work has revealed that treatment with prosaptide elicits robust GPR37 and GPR37L1, signaling in native cell types such as astrocytes but not in HEK293T cells when the receptors are overexpressed.[2] Further work is needed on GPR37 and GPR37L1 to determine why their signaling activity is so dependent on a cellular context and also to resolve the question of whether prosaptide and/or neuroprotectin D1[13] are both endogenous agonists for these receptors.

■ CONCLUSIONS

There is a growing body of evidence that dysregulation of GPR37 and GPR37L1 contributes to neurological disease. Thus, a better understanding of the normal function of these two receptors is needed. In this study, we report proteomic data analyzing global protein changes that occur in the DKO mouse brain compared to WT mouse brain. We validated S100A5 as being one of the most downregulated proteins and also found that GPR37 and GPR37L1 promote S100A5 secretion in a Ca^{2+}-dependent manner. These proteomic analyses raise many interesting questions for future studies and provide molecular insight into how loss of function of the glia-enriched receptors

https://dx.doi.org/10.1021/acs.jproteome.9b00622
J. Proteome Res. 2020, 19, 744−755

GPR37 and GPR37L1 can lead to altered seizure vulnerability and other deleterious effects.

■ ASSOCIATED CONTENT

Supporting Information

The Supporting Information is available free of charge at https://pubs.acs.org/doi/10.1021/acs.jproteome.9b00622.

Differential expression analysis of Proteomics data (DEP) with Barres Lab database, differential Expression analysis of Proteomics data (DEP) with Sharma et al. (2015) database, Differential Expression analysis of Proteomics data (DEP) with Sharma−Barres combination database with endothelial cells, antibody validation for detection of S100A5, uncropped Western blots of Figure 2A (S100A5 protein and mRNA levels are reduced in GPR37 knockout), GPR37L1 knockout, and DKO mouse brains vs. WT mouse brain, uncropped Western blots of Figure 3C (Coexpression of S100A5 with either GPR37 or GPR37L1 leads to robust secretion of S100A5 from HEK293T cells), uncropped Western blots of Figure 4A (Receptor regulation of S100A5 secretion), uncropped Western blots of Figure 4C (Receptor regulation of S100A5 secretion), uncropped Western blots of Figure 4D (Receptor regulation of S100A5 secretion),uncropped Western blots of Figure 5B (Chelation of intracellular Ca^{2+} leads to decreased S100A5 secretion from HEK239T cells), uncropped Western blots of Figure 5C (Chelation of intracellular Ca^{2+} leads to decreased S100A5 secretion from HEK239T cells), uncropped Western blots of Figure 6A (Coexpression of homologous S100A proteins with either GPR37L1 or GPR37 also leads to secretion), and uncropped Western blots of Figure 6B (Coexpression of homologous S100A proteins with either GPR37L1 or GPR37 also leads to secretion) (PDF)

Imputed WT vs. DKO whole proteome (XLSX)

Null experiment calculations for imputation of proteomic data (XLSX)

Complete lists of significantly increased and decreased proteins (XLSX)

GO ontology input and *Z* scores (XLSX)

FET heatmap values of brain cell types (all databases) (XLSX)

■ AUTHOR INFORMATION

Corresponding Author

Randy A. Hall − *Department of Pharmacology and Chemical Biology, Emory University School of Medicine, Atlanta 30322, Georgia, United States*; Phone: 404-727-3699; Email: rhall3@emory.edu

Authors

TrangKimberly Thu Nguyen − *Department of Pharmacology and Chemical Biology, Emory University School of Medicine, Atlanta 30322, Georgia, United States*; orcid.org/0000-0003-0928-2019

Eric B. Dammer − *Department of Biochemistry, Emory University School of Medicine, Atlanta 30345, Georgia, United States*

Sharon A. Owino − *Department of Pharmacology and Chemical Biology, Emory University School of Medicine, Atlanta 30322, Georgia, United States*

Michelle M. Giddens − *Department of Pharmacology and Chemical Biology, Emory University School of Medicine, Atlanta 30322, Georgia, United States*

Nora S. Madaras − *Department of Pharmacology and Chemical Biology, Emory University School of Medicine, Atlanta 30322, Georgia, United States*

Duc M. Duong − *Department of Biochemistry, Emory University School of Medicine, Atlanta 30345, Georgia, United States*

Nicholas T. Seyfried − *Department of Biochemistry, Emory University School of Medicine, Atlanta 30345, Georgia, United States*; orcid.org/0000-0002-4507-624X

Complete contact information is available at: https://pubs.acs.org/10.1021/acs.jproteome.9b00622

Notes

The authors declare no competing financial interest.

■ ACKNOWLEDGMENTS

We would like to acknowledge the Emory Proteomics Core, one of the Emory Core Facilities, for assisting with the proteomic analyses described here. This work was funded by NIH grants R21-NS91986, R21-NS106323, and R01-NS088413, and T.T.N. was supported by NIH training grant T32-GM008602.

■ ABBREVIATIONS

GPR37L1, G protein-coupled receptor 37 like-1; GPR37, G protein-coupled receptor 37; WT, wild-type; L1KO, GPR37L1-knockout; 37KO, GPR37-knockout; DKO, GPR37L1/GPR37 double knockout; MS, mass spectrometry

■ REFERENCES

(1) Cahoy, J. D.; Emery, B.; Kaushal, A.; Foo, L. C.; Zamanian, J. L.; Christopherson, K. S.; Xing, Y.; Lubischer, J. L.; Krieg, P. A.; Krupenko, S. A.; Thompson, W. J.; Barres, B. A. A transcriptome database for astrocytes, neurons, and oligodendrocytes: A new resource for understanding brain development and function. *J. Neurosci.* **2008**, *28*, 264−278.

(2) Liu, B.; Mosienko, V.; Vaccari Cardoso, B.; Prokudina, D.; Huentelman, M.; Teschemacher, A. G.; Kasparov, S. Glio- and neuroprotection by prosaposin is mediated by orphan G-protein coupled receptors GPR37L1 and GPR37. *Glia* **2018**, *66*, 2414−2426.

(3) Marazziti, D.; Golini, E.; Gallo, A.; Lombardi, M. S.; Matteoni, R.; Tocchini-Valentini, G. P. Cloning of GPR37, a gene located on chromosome 7 encoding a putative G-protein-coupled receptor, from a human frontal brain EST library. *Genomics* **1997**, *45*, 68−77.

(4) Marazziti, D.; Gallo, A.; Golini, E.; Matteoni, R.; Tocchini-Valentini, G. P. Molecular cloning and chromosomal localization of the mouse Gpr37 gene encoding an orphan G protein-coupled peptide receptor expressed in brain and testis. *Genomics* **1998**, *53*, 315−324.

(5) Smith, B. M.; Giddens, M. M.; Neil, J.; Owino, S.; Nguyen, T. T.; Duong, D.; Li, F.; Hall, R. A. Mice lacking Gpr37 exhibit decreased expression of the myelin-associated glycoprotein MAG and increase susceptibility to demyelination. *Neuroscience* **2017**, *358*, 49−57.

(6) Valdenaire, O.; Giller, T.; Breu, V.; Ardati, A.; Schweizer, A.; Richards, J. G. A new family of orphan G protein-coupled receptors predominantly expressed in the brain. *FEBS Lett.* **1998**, *424*, 193−196.

(7) Yang, H.-J.; Vainshtein, A.; Maik-Rachline, G.; Pelas, E. G protein-coupled receptor 37 is a negative regulator of oligodendrocyte differentiation and myelination. *Nat. Commun.* **2016**, *7*, 10884.

(8) Zeng, Z.; Su, K.; Kyaw, H.; Li, Y. A novel endothelin receptor type-B-like gene enriched in the brain. *Biochem. Biophys. Res. Commun.* **1997**, *233*, 559−567.

(9) Zhang, Y.; Chen, K.; Sloan, S. A.; Bennett, M. L.; Scholze, A. R.; O'Keeffe, S.; Phatnani, H. P.; Guarnieri, P.; Caneda, C.; Ruderisch, N.; Deng, S.; Liddelow, S. A.; Zhang, C.; Daneman, R.; Maniatis, T.; Barres,

B. A.; Wu, J. Q. An RNA-sequencing transcriptome and splicing database of glia, neurons, and vascular cells of the cerebral cortex. *J. Neurosci.* **2014**, *34*, 11929−11947.
(10) Rezgaoui, M.; Susens, U.; Ignatov, A.; Geldreblom, M.; Glassmeier, G.; Franke, I.; Urny, J.; Imai, Y.; Takahashi, R.; Schaller, H.C. The neuropeptide head activator is a high-affinity ligand for the orphan G-protein-coupled receptor GPR37. *J. Cell Sci.* **2006**, *119*, 542−549.
(11) Gandia, J.; Fernandez-Duenas, V.; Morato, X.; Caltabiano, G.; Gonzalez-Muniz, R.; Pardo, L.; Stagljar, I.; Ciruela, F. The Parkinson's disease-associated GPR37 receptor-mediated cytotoxicity is controlled by its intracellular cysteine-rich domain. *J. Neurochem.* **2013**, *125*, 25−35.
(12) Meyer, R. C.; Giddens, M. M.; Schaefer, S. A.; Hall, R. A. GPR37 and GPR37L1 are receptors for the neuroprotective and glioprotective factors prosaptide and prosaposin. *Proc. Natl. Acad. Sci. U.S.A.* **2013**, *110*, 9529−9534.
(13) Bang, S.; Xie, Y.-K.; Zhang, Z.-J.; Wang, Z.; Xu, Z.-Z.; Ji, R.-R. GPR37 regulates macrophage phagocytosis and resolution of inflammatory pain. *J. Clin. Invest.* **2018**, *128*, 3568−3582.
(14) Jolly, S.; Bazargani, N.; Quiroga, A. C.; Pringle, N. P.; Attwell, D.; Richardson, W. D.; Li, H. G protein-coupled receptor 37-like 1 modulates astrocyte glutamate transporters and neuronal NMDA receptors and is neuroprotective in the ischemia. *Glia* **2018**, *66*, 47−61.
(15) Lundius, E. G.; Vukojević, V.; Hertz, E.; Stroth, N.; Cederlund, A.; Hiraiwa, M.; Terenius, L.; Svenningsson, P. GPR37 protein trafficking to the plasma membrane regulated by prosaposin and GM1 gangliosides promotes cell viability. *J. Biol. Chem.* **2014**, *289*, 4660−4673.
(16) Southern, C.; Cook, J. M.; Neetoo-Isseljee, Z.; Taylor, D. L.; Kettleborough, C. A.; Merritt, A.; Bassoni, D. L.; Raab, W. J.; Quinn, E.; Wehrman, T. S.; Davenport, A. P.; Brown, A. J.; Green, A.; Wigglesworth, M. J.; Rees, S. Screening β-arrestin recruitment for the identification of natural ligands for orphan G-protein-coupled receptors. *J. Biomol. Screen* **2013**, *18*, 599−609.
(17) Coleman, J. L. J.; Ngo, T.; Schmidt, J.; Mrad, N.; Liew, C. K.; Jones, N. M.; Graham, R. M.; Smith, N. J. Metalloproteinase cleavage of the N terminus of the orphan G protein-coupled receptor GPR37L1 reduces its constitutive activity. *Sci. Signal.* **2013**, *9*, ra36.
(18) Marazziti, D.; Golini, E.; Mandillo, S.; Magrelli, A.; Witke, W.; Matteoni, R.; Tocchini-Valentini, G. P. Altered dopamine signaling and MPTP resistance in mice lacking the Parkinson's disease-associated GPR37/parkin-associated endothelin-like receptor. *Proc. Natl. Acad. Sci. U.S.A.* **2004**, *101*, 10189−10194.
(19) Marazziti, D.; Di Pietro, C.; Golini, E.; Mandillo, S.; La Sala, G.; Matteoni, R.; Tocchini-Valentini, G. P. Precocious cerebellum development and improved motor functions in mice lacking the astrocyte cilium-, patched 1-associated Gpr37l1 receptor. *Proc. Natl. Acad. Sci. U.S.A.* **2013**, *110*, 16486−16491.
(20) Giddens, M. M.; Wong, J. C.; Schroeder, J. P.; Farrow, E. G.; Smith, B. M.; Owino, S.; Soden, S. E.; Meyer, R. C.; Saunders, C.; LePichon, J. B.; Weinshenker, D.; Escayg, A.; Hall, R. A. GPR37L1 modulates seizure susceptibility: Evidence from mouse studies and analyses of a human GPR37L1 variant. *Neurobiol. Dis.* **2017**, *106*, 181−190.
(21) Dershem, R.; Raghu Metpally, R. P. R.; Jeffreys, K.; Krishnamurthy, S.; Carey, D. J.; Hershfinkel, M.; Robishaw, J. D.; Breitweiser, G. E. Rare variant pathogenicity triage and inclusion of synonymous variants improves analysis of disease associations. **2018**, bioRxiv;272955.
(22) Wang, J.; Lin, Z.-J.; Liu, L.; Xu, H.-Q.; Shi, Y.-W.; Yi, Y.-H.; He, N.; Liao, W.-P. Epilepsy-associated genes. *Seizure* **2017**, *44*, 11−20.
(23) Seyfried, N. T.; Dammer, E. B.; Swarup, V.; Nandakumar, D.; Duong, D. M.; Yin, L.; Deng, Q.; Nguyen, T.; Hales, C. M.; Wingo, T.; Glass, J.; Gearing, M.; Thambisetty, M.; Troncoso, J. C.; Geschwind, D. H.; Lah, J. J.; Levey, A. I. A multi-network approach identifies protein-specific co-expression in asymptomatic and symptomatic Alzheimer's Disease. *Cell Syst.* **2017**, *4*, 60−72.
(24) Perez-Riverol, Y.; Csordas, A.; Bai, J.; Bernal-Llinares, M.; Hewapathirana, S.; Kundu, D. J.; Inuganti, A.; Griss, J.; Mayer, G.; Eisenacher, M.; Pérez, E.; Uszkoreit, J.; Pfeuffer, J.; Sachsenberg, T.; Yılmaz, Ş.; Tiwary, S.; Cox, J.; Audain, E.; Walzer, M.; Jarnuczak, A. F.; Ternent, T.; Brazma, A.; Vizcaíno, J. A. The PRIDE database and related tools and resources in 2019: improving support for quantification data. *Nucleic Acids Res.* **2019**, *47*, D442−D450.
(25) Dai, J.; Johnson, E. C. B.; Dammer, E. B.; Duong, D. M.; Gearing, M.; Lah, J. J.; Levey, A. I.; Wingo, T. S.; Seyfried, N. T. Effects of APOE genotype on brain proteomic network and cell type changes in Alzheimer's Disease. *Front. Mol. Neurosci.* **2018**, *11*, 454.
(26) Karpievitch, Y. V.; Dabney, A. R.; Smith, R. D. Normalization and missing value imputation for label-free LC-MS analysis. *BMC Bioinf.* **2012**, *13*, S5.
(27) Tyanova, S.; Temu, T.; Sinitcyn, P.; Carlson, A.; Hein, M. Y.; Geiger, T.; Mann, M.; Cox, J. The Perseus computational platform for comprehensive analysis of (prote)omics data. *Nat. Methods* **2016**, *13*, 731−740.
(28) Sharma, K.; Schmitt, S.; Bergner, C. G.; Tyanova, S.; Kannaiyan, N.; Manrique-Hoyos, N.; Kongi, K.; Cantuti, L.; Hanisch, U.-K.; Philips, M.-A.; Rossner, M. J.; Mann, M.; Simons, M. Cell type- and brain region-resolved mouse brain proteome. *Nat. Neurosci.* **2015**, *18*, 1819−1831.
(29) Dammer, E. B.; Lee, A. K.; Duong, D. M.; Gearing, M.; Lah, J. J.; Levey, A. I.; Seyfried, N. T. Quantitative phosphoproteomics of Alzheimer's disease reveals cross-talk between kinases and small heat shock proteins. *Proteomics* **2015**, *15*, 508−519.
(30) Rao, X.; Huang, X.; Zhou, Z.; Lin, X. An improvement of the $\hat{2}$(-delta-delta CT) method for quantitative real-time polymerase chain reaction data analysis. *Biostat. Bioinforma. Biomath.* **2013**, *3*, 71−85.
(31) Zhou, X.; Sun, L.; Bastos de Oliveira, F.; Qi, X.; Brown, W. J.; Smolka, M. B.; Sun, Y.; Hu, F. Prosaposin facilitates sortilin-independent lysosomal trafficking of progranulin. *J. Cell Biol.* **2015**, *210*, 991.
(32) Zhou, X.; Sun, L.; Bracko, O.; Choi, J.W.; Jia, Y.; Nana, A.L.; Brady, O.A.; Hernandez, J.C.C.; Nishimura, N.; Seeley, W.W.; Hu, F. Impaired prosaposin lysosomal trafficking in frontotemporal lobar degeneration due to progranulin mutations. *Nat. Commun.* **2017**, *8*, 15277.
(33) Kollmann, K.; Damme, M.; Markmann, S.; Morelle, W.; Schweizer, M.; Hermans-Borgmeyer, I.; Röchert, A. K.; Pohl, S.; Lübke, T.; Michalski, J.-C.; Käkelä, R.; Walkley, S. U.; Braulke, T. Lysosomal dysfunction causes neurodegeneration in mucolipidosis II 'knock-in' mice. *Brain* **2012**, *135*, 2661−2675.
(34) Kishimoto, Y.; Hiraiwa, M.; O'Brien, J. S. Saposins: structure, function, distribution, and molecular genetics. *J. Lipid Res.* **1992**, *33*, 1255−67.
(35) Kolter, T.; Sandhoff, K. Lysosomal degradation of membrane lipids. *FEBS Lett.* **2010**, *584*, 1700−1712.
(36) Sun, Y.; Grabowski, G. A. Saposin C is required for normal resistance of acid beta-glucosidase to proteolytic degradation. *J. Biol. Chem.* **2003**, *278*, 31918−31923.
(37) Di Pietro, C.; Marazziti, D.; La Sala, G.; Abbaszadeh, Z.; Golini, E.; Matteoni, R.; Tocchini-Valentini, G. P. Primary cilia in the murine cerebellum and in mutant models of medulloblastoma. *Cell. Mol. Neurobiol.* **2017**, *37*, 145−154.
(38) Imai, Y.; Soda, M.; Hatakeyama, S.; Akagi, T.; Hashikawa, T.; Nakayama, K.-I.; Takahashi, R. CHIP is associated with Parkin, a gene responsible for familial Parkinson's Disease, and enhances its ubiquitin ligase activity. *Mol. Cell* **2002**, *10*, 55−67.
(39) Marenholz, I.; Heizmann, C. W.; Fritz, G. S100 proteins in mouse and man: from evolution to function and pathology (including an update of the nomenclature). *Biochem. Biophys. Res. Commun.* **2004**, *322*, 1111−1122.
(40) Iacobas, D. A.; Iacobas, S.; Nebieridze, N.; Velisek, L.; Veliskova, J. Estrogen protects neurotransmission transcriptome during status epilepticus. *Front. Neurosci.* **2018**, *12*, 332.
(41) Ishihara, Y.; Itoh, K.; Tanaka, M.; Tsuji, M.; Kawamoto, T.; Kawato, S.; Vogel, C. F. A.; Yamazaki, T. Potential of 17β-estradiol

synthesis in the brain and elongation of seizure latency through dietary supplementation with docohexaenoic acid. *Sci. Rep.* **2017**, *7*, 6268.
(42) Mostacci, B.; Esposto, R.; Lello, S.; Bisulli, F.; Licchetta, L.; Tinuper, P. Estrogen-related seizure exacerbation following hormone therapy for assisted reproduction in women with epilepsy. *Seizure* **2018**, *61*, 200−202.
(43) Sarfi, M.; Elahdadi Salmani, M.; Goudarzi, I.; Lashkar Boluki, T.; Abrari, K. Evaluating the role of astrocytes on β-estradiol effect on seizures of Pilocarpine epileptic model. *Eur. J. Pharmacol.* **2017**, *797*, 32−38.
(44) Sato, S. M.; Woolley, C. S. Acute inhibition of neurosteroid estrogen synthesis suppresses status epilepticus in an animal model. *Elife* **2016**, *5*, No. e12917.
(45) Ramanujam, B.; Arora, A.; Malhotra, V.; Dash, D.; Mehta, S.; Tripathi, M. A case of recurrent status epilepticus and successful management with progesterone. *Epileptic Disord.* **2016**, *18*, 101−105.
(46) Wu, Y. V.; Burnham, W. M. The anti-seizure effects of IV 5α-dihydroprogesterone on amygdala-kindled seizures in rats. *Epilepsy Res.* **2018**, *146*, 132−136.
(47) Schäfer, B. W.; Fritschy, J.-M.; Murmann, P.; Troxler, H.; Durussel, I.; Heizmann, C. W.; Cox, J. A. Brain S100A5 is a novel calcium-, zinc-, and copper ion-binding protein of the EF-hand superfamily. *J. Biol. Chem.* **2000**, *275*, 30623−30630.
(48) Camby, I.; Nagy, N.; Lopes, M. B.; Schafer, B. W.; Maurage, C. A.; Ruchoux, M. M.; Murmann, P.; Pochet, R.; Heizmann, C. W.; Brotchi, J.; Salmon, I.; Kiss, R.; Decaestecker, C. Supratentorial pilocytic astrocytomas, astrocytomas, anaplastic astrocytomas and glioblastomas are characterized by a differential expression of S100 proteins. *Brain Pathol.* **1999**, *9*, 1−19.
(49) Camby, I.; Lefranc, F.; Titeca, G.; Neuci, S.; Fastrez, M.; Dedecken, L.; Schafer, B. W.; Brotchi, J.; Heizmann, C. W.; Pochet, R.; Salmon, I.; Kiss, R.; Decaestecker, C. Differential expression of S100 calcium-binding proteins characterizes distinct clinical entities in both WHO grade II and III astrocytic tumors. *Neuropathol. Appl. Neurobiol.* **2000**, *26*, 76−90.
(50) Dmytriyeva, O.; Panktratova, S.; Owczarek, S.; Sonn, K.; Soroka, V.; Ridley, C.M.; Marsolais, A.; Lopez-Hoyos, M.; Ambartsumian, N.; Lukanidin, E.; Bock, E.; Berezin, V.; Kiryushko, D. The metastasis-promoting S100A4 protein confers neuroprotection in brain injury. *Nat. Commun.* **2012**, *3*, 1197.
(51) Bartkowska, K.; Swiatek, I.; Aniszewska, A.; Jurewicz, E.; Turlejski, K.; Filipek, A.; Djavadian, R. L. Stress-dependent changes in the CacyBP/SIP interacting protein S100A6 in the mouse brain. *PLoS One* **2016**, *12*, No. e0169760.
(52) Donato, R.; Sorci, G.; Giambanco, I. S100A6 protein: functional roles. *Cell. Mol. Life Sci.* **2017**, *74*, 2749−2760.
(53) Leśniak, W.; Wilanowski, T.; Filipek, A. S100A6—focus on recent developments. *Biol. Chem.* **2017**, *398*, 1087−1094.
(54) Kubista, H.; Donato, R.; Hermann, A. S100 calcium binding protein affects neuronal electrical discharge activity by modulation of potassium currents. *Neuroscience* **1999**, *90*, 493−508.
(55) Melani, R.; Rebaudo, R.; Balestrino, M.; Cupello, A.; Haglid, K.; Hydèn, H. Involvement of S-100 protein in anoxic long-term potentiation. *Brain Res.* **1999**, *840*, 171−174.
(56) Nikitin, V. P.; Kozyrev, S. A.; Shevelkin, A. V. The effects of antibodies against proteins of the S100 group on neuron plasticity in sensitized and non-sensitized snails. *Neurosci. Behav. Physiol.* **2002**, *32*, 25−31.
(57) Nishiyama, H.; Knöpfel, T.; Endo, S.; Itohara, S. Glial protein S100B modulates long-term neuronal synaptic plasticity. *Proc. Natl. Acad. Sci. U.S.A.* **2002**, *99*, 4037−42.
(58) Rebaudo, R.; Melani, R.; Balestrino, M.; Cupello, A.; Haglid, K.; Hydè, H. Antiserum against S-100 protein prevents long-term potentiation through a cAMP-related mechanism. *Neurochem. Res.* **2000**, *25*, 541−545.
(59) Sakatani, S.; Seto-Ohshima, A.; Shinohara, Y.; Yamamoto, Y.; Yamamoto, H.; Itohara, S.; Hirase, H. Neural-activity-dependent release of S100B from astrocytes enhances kainite-induced gamma oscillations *in vivo*. *J. Neurosci.* **2008**, *28*, 10928−10936.
(60) Davey, G. E.; Murmann, P.; Heizmann, C. W. Intracellular Ca^{2+} and Zn^{2+} levels regulate the alternative cell density-dependent secretion of S100B in human glioblastoma cells. *J. Biol. Chem.* **2001**, *276*, 30819−30826.
(61) Gerlach, R.; Demel, G.; König, H.-G.; Gross, U.; Prehn, J. H. M.; Raabe, A.; Seifert, V.; Kögel, D. Active secretion of S100B from astrocytes during metabolic stress. *Neuroscience* **2006**, *141*, 1697−1701.
(62) Guerra, M.; Tortorelli, L. S.; Galland, F.; Da Ré, C.; Negri, E.; Engelke, D. S.; Rodrigues, L.; Leite, M. C.; Gonçalves, C.-A. Lipopolysaccharide modulates astrocytic S100B secretion: a study in cerebrospinal fluid and astrocyte cultures from rats. *J. Neuroinflammation* **2011**, *8*, 128.
(63) Tramontina, A. C.; Tramontina, F.; Bobermin, L. D.; Zanotto, C.; Souza, D. F.; Leite, M. C.; Nardin, P.; Gottfried, C.; Gonçalves, C.-A. Secretion of S100B, an astrocyte-derived neurotrophic protein, is stimulated by fluoxetine via a mechanism independent of serotonin. *Prog. Neuro Psychopharmacol. Biol. Psychiatry* **2008**, *32*, 1580−1583.
(64) Kathir, K. M.; Ibrahim, K.; Rajalingam, D.; Prudovsky, I.; Yu, C.; Kumar, T. K. S. S100A13-lipid interactions-role in the non-classical release of the acidic fibroblast growth factor. *Biochim. Biophys. Acta, Biomembr.* **2007**, *1768*, 3080−3089.
(65) Zolese, G.; Tangorra, A.; Curatola, G.; Giambanco, I.; Donato, R. Interaction of S-100b protein with cardiolipin vesicles as monitored by electron spin resonance, pyrene fluorescence and circular dichroism. *Cell Calcium* **1988**, *9*, 149−157.
(66) Bhattacharya, S.; Bunick, C. G.; Chazin, W. J. Target selectivity in EF-hand calcium binding proteins. *Biochim. Biophys. Acta, Mol. Cell Res.* **2004**, *1742*, 69−79.
(67) Zimmer, D. B.; Weber. The calcium-dependent interaction of S100B with its target protein targets. *Cardiovasc. Psychiatry Neurol.* **2010**, *2010*, 728052.
(68) Velásquez, E.; Nogueira, F. C. S.; Velásquez, I.; Schmitt, A.; Falkai, P.; Domont, G. B.; Martins-de-Souza, D. Synaptosomal proteome of the orbitofrontal cortex from Schizophrenia patients using quantitative label-free and iTRAQ-based shotgun proteomics. *J. Proteome Res.* **2017**, *16*, 4481−4494.
(69) Eshraghi, M.; Gombar, R.; De Repentigny, Y.; Vacratsis, P. O.; Kothary, R. Pathologic alterations in the proteome of synaptosomes from a mouse model of Spinal Muscular Atrophy. *J. Proteome Res.* **2019**, *18*, 3042−3051.
(70) Kong, D.; Tian, X.; Li, Y.; Zhang, S.; Cheng, Y.; Huo, L.; Ma, H.; Yang, Z.; Ren, L.; Zhang, M.; Zhang, W. Revealing the inhibitory effect of ginseng on mitochondrial respiration through synaptosomal proteomics. *Proteomics* **2018**, *18*, 1700354.
(71) Donato, R. The specific interaction of S-100 protein with synaptosomal particulate fraction. Evidence for the formation of a tight complex between S-100 and its binding sites. *J. Neurochem.* **1981**, *36*, 532−537.
(72) Curatola, G.; Mazzanti, L.; Ferretti, G.; Donato, R. S 100 protein-induced changes in the physical state of synaptosomal particulate fractions as monitored by spin labels. *Arch. Biochem. Biophys.* **1985**, *240*, 435−445.
(73) Donato, R.; Michetti, F. Specific binding sites for S-100 protein in isolated brain nuclei. *J. Neurochem.* **1981**, *36*, 1698−1705.
(74) Starostina, M. V.; Nikolaenkova, A. A.; Malup, T. K.; Korochkin, L. I.; Sviridov, S. M. Quantitative assay of S-100 protein in mouse brain cortex synaptosomes. *Cell. Mol. Neurobiol.* **1993**, *13*, 677−691.
(75) Starostina, M. V.; Sviridov, S. M. Quantitative determination of neurospecific protein S-100 in mouse brain cortical synaptosomes. *Biokhimiia* **1981**, *46*, 2030−2042.
(76) Cocchia, D.; Pansera, F.; Palumbo, A.; Donato, R. Immunocytochemical localization of S-100 protein binding sites in synaptosomal fractions and subfractions. *Cell. Mol. Neurobiol.* **1982**, *2*, 265−276.

https://dx.doi.org/10.1021/acs.jproteome.9b00622
J. Proteome Res. 2020, 19, 744−755